energies

MDPI

Article

# A Comparative Study of Using Polarization Curve Models in Proton Exchange Membrane Fuel Cell Degradation Analysis

**Chen Zhang [1], Wen Li [2], Mingruo Hu [3], Xiaofang Cheng [2], Kai He [1] and Lei Mao [1,*]**

1 Department of Precision Machinery and Precision Instrumentation, University of Science and Technology of China, Hefei 230026, China; zhang985@mail.ustc.edu.cn (C.Z.); hk2014@mail.ustc.edu.cn (K.H.)
2 Department of Thermal Science and Energy Engineering, University of Science and Technology of China, Hefei 230026, China; liwen96@mail.ustc.edu.cn (W.L.); xfcheng@ustc.edu.cn (X.C.)
3 School of Mechanical Engineering, Shanghai Jiao Tong University, Shanghai 200240, China; mingruohu@sjtu.edu.cn
* Correspondence: leimao82@ustc.edu.cn

Received: 23 June 2020; Accepted: 20 July 2020; Published: 22 July 2020

**Abstract:** In this paper, a systematic study is carried out to compare the performance of various V-I models at both normal and faulty conditions, in terms of simulating proton exchange membrane fuel cell (PEMFC) behavior and analyzing the corresponding degradation process. In the analysis, the simulation accuracy of V-I models, including overall behavior simulation and the simulation of different PEMFC losses, is investigated. Results show that compared to the other V-I models, the V-I model using exponential function for mass transport loss and considering open circuit voltage (OCV) at zero current can provide the best simulation performance, with an overall root mean square error (RMSE) of about 0.00279. Furthermore, the performance of these V-I models in analyzing PEMFC degradation process is also studied. By investigating the evolution of PEMFC losses during the degradation, the effectiveness of these models in interpreting PEMFC degradation mechanisms can be clarified. The results show that, besides the simulation accuracy, different interpretations may be provided from different models; this further confirms the necessity of comparative study. Moreover, the effectiveness of different V-I models in identifying PEMFC abnormal performance at two faulty scenarios is investigated. The results demonstrate that, among different V-I models, the model using an exponential function for mass transport loss and considering OCV at zero current can provide more accurate simulation and reasonable interpretation regarding PEMFC internal behavior.

**Keywords:** PEMFC; V-I model; fitting accuracy; degradation analysis

## 1. Introduction

In recent years, with the continuous depletion of fossil fuel resources, as well as harmful greenhouse gas emissions to the environment, the hydrogen and fuel cell technology has received more attention. As a clean and efficient way of energy utilization, fuel cell, especially proton exchange membrane fuel cell (PEMFC), can convert chemical energy into electrical energy, with several characteristics, such as environment friendly, high energy conversion efficiency, low noise, low temperature operation, etc. [1] This makes PEMFC system equipped at many fields, including transportation, military and space applications, and so on.

However, further commercialization of the PEMFC system is prevented by its limited reliability and durability. One of the main reasons is that PEMFC aging phenomena and corresponding degradation mechanisms, especially at dynamic operating conditions such as automotive application, have not been fully clarified. This brings great difficulty of taking appropriate mitigation strategies to extend its lifetime. Therefore, a set of researches has been devoted to PEMFC degradation analysis.

Among various techniques, polarization curves (V-I curves) are widely used in analyzing the PEMFC degradation process. By investigating variations in V-I model parameters during PEMFC operation, different losses, including activation, Ohmic and mass transport losses, can be evaluated [2]. Several studies have been performed using V-I curves in PEMFC analysis and improvement. Effects of operating parameters, geometric parameters and material parameters on the V-I curves were investigated in [3], from which the PEMFC design could be optimized to improve its performance. Furthermore, the effects of PEMFC properties on V-I curves were also studied in [4], and the results demonstrated that PEMFC performance could be improved by increasing the temperature, active area, membrane exchange capacity and decreasing the membrane resistance. In [5], the variation law between V-I model parameters and operating conditions was established, and a predictive model was developed. Moreover, the variation of V-I model parameters, including reversible cell voltage, Tafel slope and Ohmic resistance, was studied under strengthened road vibrating condition in [6]. In [7], over-potential losses in V-I curves were separated, and the contribution of each loss to PEMFC performance degradation was obtained [8], and the PEMFC degradation mechanism was evaluated by analyzing variation of V-I model parameters relating to different losses [9–12]. More recently, Vuppala et al. developed a two-phase PEMFC model, to optimize the design of membrane electrode assembly (MEA). In the analysis, a response surface method was used for optimization, and optimization results were validated using V-I curves [13].

From the above studies, it can be concluded that PEMFC behavior can be analyzed with V-I models, and results can be used to design appropriate strategies for minimizing PEMFC losses and improving its performance [14].

However, although V-I models are widely used in analyzing the PEMFC degradation process, different expressions of V-I models have been proposed in previous studies. In [15], a V-I model was proposed to evaluate effects of gas pressure and membrane thickness on cell resistance, and the mass transport term of a proposed model could be correlated to electrode properties. Danilov and Tade developed a new V-I model for estimating cathodic and anodic charge coefficients simultaneously [16]. In [17], a different V-I model was developed, which showed excellent performance in fitting V-I data at different temperature, pressure and oxygen/inert gas compositions. Guinea et al. developed another V-I model considering electron leakage current density, such that accurate fitting performance could be achieved with rotary optimization and gradient optimization methods [18]. In [19], a new semi-empirical V-I model considering PEMFC behavior at zero current density was constructed, which showed good agreement between experimental data and model simulation.

It can be observed from above studies that different V-I models have been proposed for PEMFC analysis, including the analysis of PEMFC degradation. This brings great challenge in selecting proper V-I model at practical PEMFC applications, as performance bias can be provided with different V-I models. Therefore, it is urgently required to compare the performance of various V-I models in PEMFC degradation analysis at different conditions, from which pros and cons of V-I models can be better clarified.

In this study, a comparative study is performed to evaluate the effectiveness of commonly used V-I models in PEMFC degradation analysis at different conditions, including normal operation and faulty scenarios. In the analysis, the model simulation accuracy, interpretation of PEMFC degradation process, and identification of PEMFC abnormal behavior are systematically investigated. Based on the findings, the pros and cons of these V-I models can be better clarified, which will be beneficial in selecting appropriate V-I models for PEMFC degradation analysis. The novelty of this work lies in that a systematic study is performed to compare the effectiveness of widely used V-I models in PEMFC degradation analysis, while in existing studies, different V-I models have been applied for such purpose, but their performance has not been compared. As variations in simulation accuracy and interpretation of PEMFC degradation can be provided with different V-I models, it is difficult to select appropriate V-I models at practical PEMFC applications for degradation analysis. Therefore, this study can bridge the gap between various V-I models available for PEMFC degradation analysis and proper model selection at practical PEMFC applications. Moreover, this study clarifies the pros and cons of V-I models in identifying PEMFC behavior at faulty scenarios, which can be used as a guideline for selecting an appropriate V-I model in the PEMFC fault diagnosis.

The paper is organized as follows. In Section 2, the commonly used V-I models are presented and divided into different categories, and a representative model from each category is selected for the following analysis. Section 3 presents the comparative study of selected V-I models performance in PEMFC degradation analysis at normal operation condition. In Section 4, the effectiveness of V-I models in PEMFC analysis at two faulty scenarios, including flooding and dehydration, is investigated. From the results, conclusions are made in Section 5.

## 2. Description of PEMFC V-I models

As described in Section 1, various V-I models have been proposed and used in PEMFC degradation analysis, where different expressions of PEMFC activation and mass transport losses are used. In this analysis, the V-I models used in simulating PEMFC behavior and analyzing its degradation are listed below. More details can be found in corresponding references.

Reference [15]:

$$V = E - \Delta V_a - \Delta V_o - \Delta V_m = E - A\ln\left(\frac{i}{i_0}\right) - iR + \alpha i^k \ln(1 - \beta i) \tag{1}$$

Reference [16]:

$$V = E - \Delta V_a - \Delta V_o - \Delta V_m = E - A\ln\left(\frac{i}{i_0}\right) - iR - B\ln\left(1 - \frac{i}{i_L}\right), \tag{2}$$

Reference [17]:

$$V = E - \Delta V_a - \Delta V_o - \Delta V_m = E - A\ln\left(\frac{i}{i_0}\right) - iR - m\exp(ni), \tag{3}$$

Reference [18]:

$$V = E - \Delta V_a - \Delta V_o - \Delta V_m = E - A\ln\left(\frac{i + i_n}{i_0}\right) - R(i + i_n) + B\ln\left(1 - \frac{i + i_n}{i_L}\right) \tag{4}$$

Reference [19]:

$$V = E - \Delta V_a - \Delta V_o - \Delta V_m = E - A\ln(1 - C_1 i) - iR - m[1 - \exp(ni)]. \tag{5}$$

From above equations, it can be observed that, in order to simulate PEMFC behaviors, three terms are always used in V-I models for representing activation, Ohmic, and mass transport losses, respectively, but the expressions of activation and mass transport losses may vary in different V-I models. With further analysis, the above V-I models can be divided into two categories. In the 1st group, logarithm functions are used to express both activation and mass transport losses, such as Equations (1), (2) and (4), while in the second group, logarithm and exponential functions are used to express activation and mass transport losses, respectively, like Equations (3) and (5).

In order to simplify the analysis complexity while keeping genericity, each V-I model is selected from a category in the following analysis, including Equations (2) and (3). It should be mentioned that the specific parameters, like '$i^k$' in Equation (1) and '$i_n$' in Equation (4), are not used herein, since these parameters are added in previous studies to improve model simulation performance at specific applications. For example, compared to Equation (2), parameter '$\alpha i^k$' in Equation (1) acts as an 'amplification term', and 'k' is a dimensionless number. With these extra parameters, the effect of a specific parameter on PEMFC performance can be investigated. As the focus of this study is comparing simulation performance of widely used V-I models and their effectiveness in analyzing PEMFC behavior at different states, the influence of specific model parameters is not included in this study. Therefore, only general terms are used in our work, such that the variation of different models can be better clarified.

Moreover, it is noted that, although Equation (5) has a similar expression to Equation (3), it is proposed such that the cell voltage can be exactly the same as open circuit voltage (OCV) at zero current density. Thus, in this study, Equation (5) is also included in the following analysis, so that the effect of considering zero current density behavior in a V-I model can be clarified.

Therefore, in the following analysis, the performance of three V-I models, i.e., Equations (2), (3) and (5), in simulating PEMFC behavior and analyzing PEMFC degradation at different operation conditions will be investigated.

## 3. Comparative Study of V-I models in PEMFC Degradation Analysis at Normal Condition

In this section, the performance of three V-I models in analyzing PEMFC degradation process at a normal operating condition will be investigated. The simulation accuracy of three V-I models is firstly compared, then PEMFC degradation mechanism is analyzed by studying the evolution of PEMFC losses obtained with these V-I models.

### *3.1. Description of Tested PEMFC System*

The benchmark data used in IEEE PHM 2014 Data Challenge are selected in the analysis [20]. The tested PEMFC stack is assembled in FCLAB (shown in Figure 1a), which consists of five cells, with each having active area of 100 $cm^2$. The nominal current density and maximal current density of the tested PEMFC system are 0.7 $A{\cdot}cm^{-2}$ and 1 $A{\cdot}cm^{-2}$, respectively. Table 1 lists the operating parameters used in the test.

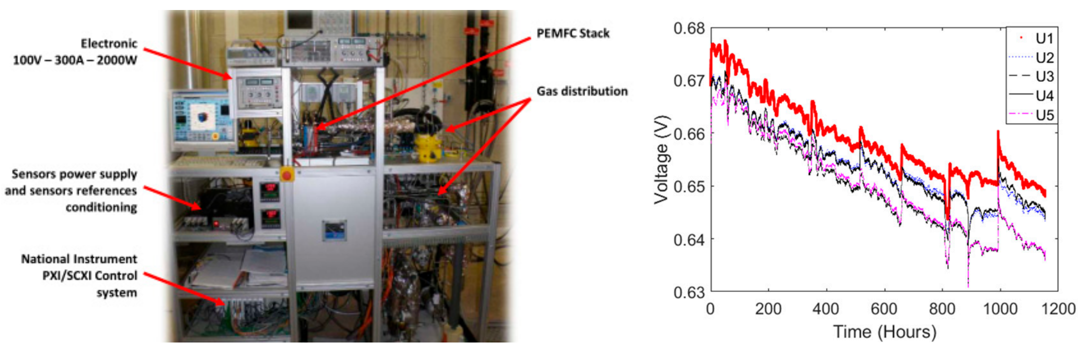


(a) (b)

**Figure 1.** Aging test of PEMFC stack. (**a**) PEMFC stack test bench [20]; (**b**) Cells voltages during the test.

**Table 1.** Proton exchange membrane fuel (PEMFC) operating parameters.

| Parameter | Value |
|---|---|
| $H_2$ /air temperature | 28 °C/42 °C |
| Cooling water temperature | 54 °C |
| Air flow | 23 $L{\cdot}min^{-1}$ |
| $H_2$ flow | 4.8 $L{\cdot}min^{-1}$ |
| Gas pressure | 1.3 bars |
| Fuel cell current | 70 A |

As shown in Table 1, the PEMFC stack is operated at a steady state with a constant current density of 0.7 $A{\cdot}cm^{-2}$, and the voltages of five cells during the test is shown in Figure 1b. It can be seen that in the test, variations in voltage amplitude are observed from cells at different positions within the stack; this is due to the unbalanced distribution of reactant gas and cooling water [21]. However, since the main focus of this study is to analyze the PEMFC behavior variation in the degradation process, and five cells show an almost identical degradation trend, the voltage variation between the cells is not considered in this study. Therefore, the average cell voltage is used in the following analysis.

Moreover, in order to analyze the PEMFC degradation process during the operation, V-I curves are collected with certain interval (about a week) during the test, i.e. at 0 h, 48 h, 185 h, 348 h, 515 h, 658 h, 823 h, 991 h, respectively. Figure 2 depicts the collected V-I curves during the PEMFC operation.

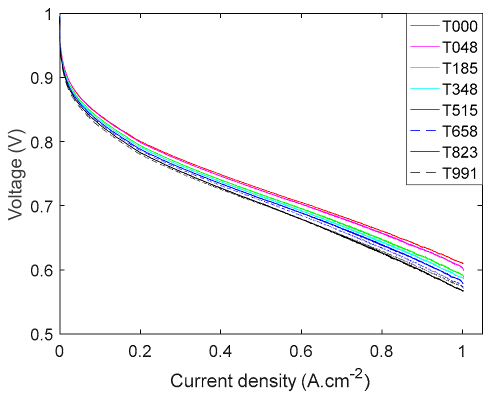


**Figure 2.** Collected V-I curves during PEMFC test.

It can be seen from Figure 2 that PEMFC performance decays gradually during the test. The only exception is that, at 991 h, where reduced mass transport loss is observed. The reason is that a voltage drop at 991 h is larger than the pre-defined failure threshold, thus, the PEMFC stack is regarded as degraded at that time [22], which will cause PEMFC abnormal behavior—this will be further investigated in Section 3.2.

As shown in Figure 2, although the degradation trend can be observed from collected V-I curves, the PEMFC degradation mechanisms, such as variations in different PEMFC losses, cannot be obtained directly with V-I curves.

## *3.2. Effectiveness of V-I models in Analyzing PEMFC Degradation*

Before analyzing PEMFC degradation using three V-I models described in Section 2, the simulation accuracy of these models is firstly compared, as the accurate simulation is the key for PEMFC reliable analysis. Table 2 lists the root mean square error (RMSE) between collected V-I curves and three V-I models, which is calculated using Equation (6). It should be noted that the same fitting technique (curve fitting toolbox in MatlabR2018) is used for three V-I models.

$$\mathrm{RMSE} = \sqrt{\frac{\sum_{i=1}^{N}\left(y_i - \overline{y_i}\right)^2}{N}}, \tag{6}$$

where $y_i$ is ith test data of aging test, $\overline{y_i}$ is ith fitting data of three V-I models, N is the number of measurement data.

**Table 2.** Fitting accuracy of three V-I models.

| Model No. | T000 | T048 | T185 | T348 | T515 | T658 | T823 | T991 |
|---|---|---|---|---|---|---|---|---|
| Equation (2) | 0.00337 | 0.00355 | 0.00339 | 0.00377 | 0.00355 | 0.00387 | 0.00332 | 0.00323 |
| Equation (3) | 0.00337 | 0.00326 | 0.00315 | 0.00326 | 0.00337 | 0.00319 | 0.00313 | 0.00311 |
| Equation (5) | 0.00236 | 0.00260 | 0.00291 | 0.00299 | 0.00301 | 0.00295 | 0.00277 | 0.00277 |

From Table 2, it can be seen that, with the same fitting technique, all three V-I models can simulate actual PEMFC performance with good quality (the maximum RMSE is below 0.004), indicating that reliable simulation performance can be obtained with these three widely used V-I models. More specifically, Equation (5) can provide the best simulation accuracy; this is reasonable, as Equation (5) can better simulate PEMFC behavior at zero current density, while with the other two V-I models, OCV cannot be achieved at zero current density. Moreover, Equation (3) has better simulation accuracy than that with Equation (2), indicating that the use of exponential function for mass transport loss can provide better simulation performance.

Furthermore, the simulation accuracy of three V-I models at different current densities is also investigated, which can be used to evaluate model simulation performance to different PEMFC losses, as shown in Figure 3. It should be noted that the absolute error between fitted value and actual measurement is used in the analysis (y-axis in Figure 3). Moreover, four V-I curves are depicted herein to represent the simulation accuracy at the beginning, middle and end of the experiment, respectively.

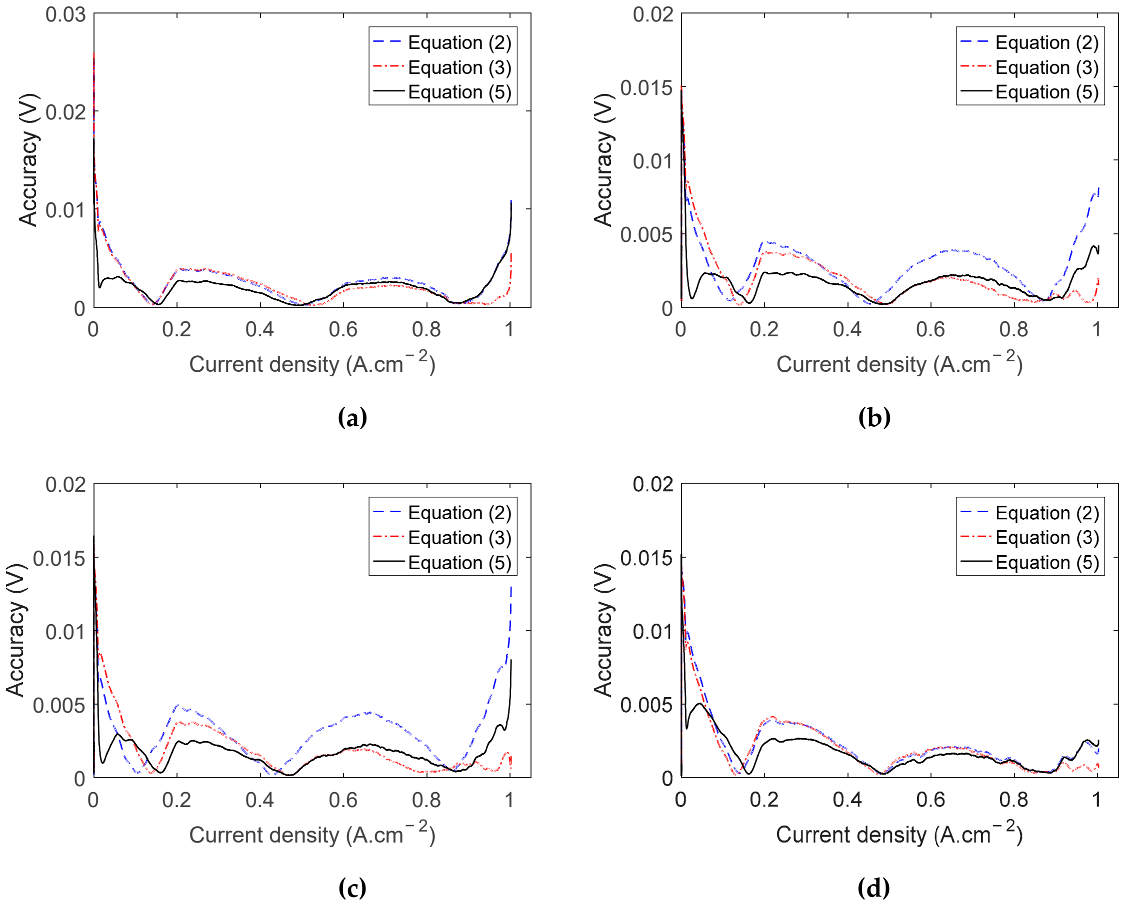


**Figure 3.** Simulation accuracy of three V-I models at different current densities collected at (**a**) 48 h; (**b**) 348 h; (**c**) 658 h; (**d**) 991 h.

Moreover, in order to better illustrate the model variation, the V-I curve is divided into 3 segments to express activation, Ohmic, and mass transport terms, respectively, as shown in Figure 4a. With such segmentation, the fitting accuracy of each term can be expressed, and its average values are listed in Table 3.

It can be seen from Figure 3 that the fitting error at low current density range (below about 0.1 A$\cdot$cm$^{-2}$) is clearly higher with Equations (2) and (3); this is due to the poor simulation performance at zero current density of these models. This error can be reduced significantly by modifying the model to account for PEMFC behavior at zero current density using Equation (5). Moreover, at Ohmic loss range (between about 0.18 A·cm$^{-2}$ and 0.75 A·cm$^{-2}$), Equation (5) can still provide a better fitting performance than those from Equations (2) and (3). However, at mass transport range with current density higher than 0.9 A·cm$^{-2}$, the best fitting can be obtained with Equation (3), while Equation (2) provides the worst simulation performance.

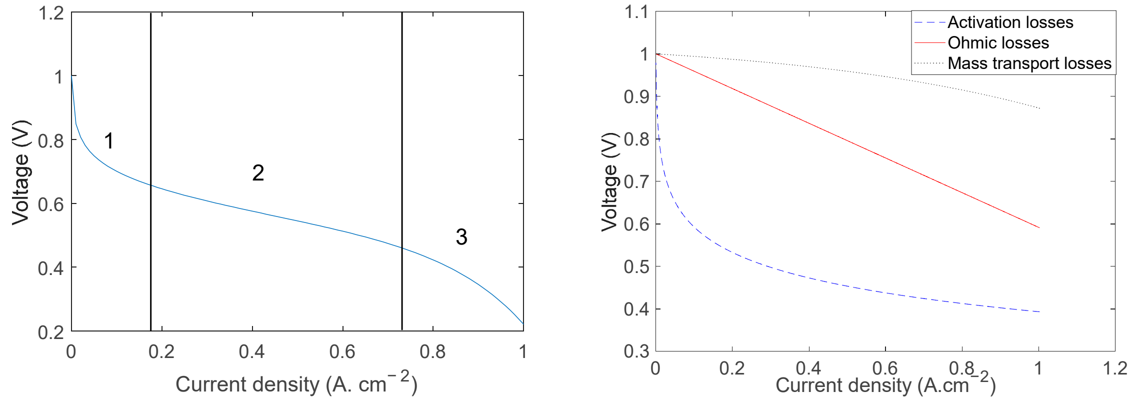


**(a)** **(b)**

**Figure 4.** (**a**) A typical PEMFC V-I curve (1: activation loss; 2: Ohmic loss; 3: mass transport loss); (**b**) three different losses' functions.

**Table 3.** Mean fitting accuracy of three terms in V-I curve using different models.

| Mean Fitting Accuracy (mV) | V-I Model | T000 | T048 | T185 | T348 | T515 | T658 | T823 | T991 |
|---|---|---|---|---|---|---|---|---|---|
| Activation | Equation (2) | 6.3 | 6.5 | 6.7 | 3.5 | 4.9 | 2.8 | 3.3 | 2.8 |
| | Equation (3) | 6.2 | 6.3 | 6.5 | 3.8 | 4.3 | 3.1 | 3.2 | 2.7 |
| | Equation (5) | 3.4 | 3.7 | 3.8 | 3.6 | 3.9 | 2.8 | 2.7 | 2.3 |
| Ohmic | Equation (2) | 2 | 2.1 | 1.9 | 2.4 | 1.9 | 2.7 | 1.8 | 1.8 |
| | Equation (3) | 1.9 | 1.9 | 1.7 | 1.7 | 2.0 | 1.6 | 1.6 | 1.8 |
| | Equation (5) | 1.5 | 1.6 | 1.9 | 1.5 | 1.4 | 1.4 | 1.3 | 1.4 |
| Mass transport | Equation (2) | 2.6 | 3.2 | 2.3 | 4.6 | 1.4 | 5.5 | 1.6 | 1.7 |
| | Equation (3) | 5.1 | 0.8 | 0.9 | 0.7 | 1.7 | 0.9 | 0.8 | 0.7 |
| | Equation (5) | 2.5 | 3.2 | 3.9 | 2.3 | 1.7 | 2.5 | 1.4 | 1.7 |

Higher simulation error of Equation (2) at mass transport range is further studied by investigating the PEMFC V-I curve, which is depicted in Figure 4a. It can be seen that a typical V-I curve contains three parts for activation, Ohmic, and mass transport terms, respectively. On the other side, Figure 4b shows three functions used for V-I curve simulation, including linear, logarithmic, and exponential functions. It can be found that, since the shape of mass transport loss is more similar to exponential function, the use of a logarithmic function for mass transport simulation will provide larger errors.

Furthermore, the PEMFC degradation process is investigated using three V-I models. In the analysis, with the above fitting process, model parameters of three V-I models can be obtained with each collected V-I curve. Tables 4–6 list the model parameters from three V-I models. With obtained model parameters from Equations (2), (3) and (5), three different PEMFC losses, including activation, Ohmic and mass transport losses, are calculated. From the results, the evolution of three PEMFC losses during the test can be illustrated, which is depicted in Figure 5.

**Table 4.** Fitted model parameters in Equation (2).

| Equation (2) | R | A | $i_0$ | B | $i_L$ |
|---|---|---|---|---|---|
| T000 | 0.1809 | 0.02309 | $2.16 \times 10^{-4}$ | −0.4831 | 55.1 |
| T048 | 0.1642 | 0.02363 | $2.35 \times 10^{-4}$ | −0.1102 | 4.474 |
| T185 | 0.1692 | 0.02454 | $2.383 \times 10^{-4}$ | −0.02055 | 0.7657 |
| T348 | 0.1756 | 0.02345 | $1.87 \times 10^{-4}$ | −96.09 | 3448 |
| T515 | 0.1781 | 0.02416 | $1.167 \times 10^{-4}$ | −0.01258 | 1.102 |
| T658 | 0.1795 | 0.02357 | $1.689 \times 10^{-4}$ | −8.438 | 269.3 |
| T823 | 0.1827 | 0.02403 | $1.525 \times 10^{-4}$ | −0.02178 | 1.23 |
| T991 | 0.185 | 0.02427 | $1.367 \times 10^{-4}$ | −0.01133 | 1.143 |

**Table 5.** Fitted model parameters in Equation (3).

| Equation (3) | R | A | $i_0$ | m | n |
|---|---|---|---|---|---|
| T000 | 0.1847 | 0.02316 | $2.43 \times 10^{-4}$ | $2.429 \times 10^{-3}$ | 0.6321 |
| T045 | 0.189 | 0.02379 | $2.458 \times 10^{-4}$ | $3.145 \times 10^{-7}$ | 10.15 |
| T185 | 0.1915 | 0.02453 | $2.437 \times 10^{-4}$ | $1.95 \times 10^{-6}$ | 8.674 |
| T348 | 0.196 | 0.02383 | $1.9 \times 10^{-4}$ | $2.086 \times 10^{-7}$ | 11.1 |
| T515 | 0.1965 | 0.02398 | $1.757 \times 10^{-4}$ | $3.509 \times 10^{-7}$ | 10.76 |
| T658 | 0.2003 | 0.02409 | $1.721 \times 10^{-4}$ | $7.991 \times 10^{-7}$ | 9.999 |
| T823 | 0.2085 | 0.02384 | $1.518 \times 10^{-4}$ | $1.541 \times 10^{-6}$ | 9.274 |
| T991 | 0.2012 | 0.02406 | $1.355 \times 10^{-4}$ | $1.834 \times 10^{-6}$ | 8.751 |

**Table 6.** Fitted model parameters in Equation (5).

| Equation (5) | R | A | $C_1$ | m | n |
|---|---|---|---|---|---|
| T000 | 0.1043 | 0.02869 | 1540 | 0.1169 | 0.4701 |
| T045 | 0.1075 | 0.0288 | 1560 | 0.1088 | 0.4996 |
| T185 | 0.1073 | 0.02736 | 2243 | 0.1796 | 0.3788 |
| T348 | 0.1134 | 0.03188 | 1232 | 0.03 | 1.187 |
| T515 | 0.05217 | 0.03332 | 1192 | 0.08399 | 0.9221 |
| T658 | 0.1091 | 0.0318 | 1440 | 0.03547 | 1.181 |
| T823 | 0.1154 | 0.03076 | 1861 | 0.03183 | 1.288 |
| T991 | 0.1283 | 0.02961 | 2530 | 0.02609 | 1.235 |

It can be found from Figure 5 that, from all three V-I models, activation loss makes the most contribution to the PEMFC losses, and mass transport loss takes the smallest portion among three losses. The reason is that mass transport loss is mainly due to the impedance of reactants transport to catalyst sites, which causes the loss of gas-phase permeability in the porous layers of PEMFC. Based on the previous studies [23–27], large mass transport loss is usually associated with poor water management, such as cell flooding at high current density range, thus, its contribution at lower current density (0.7 A·cm$^{-2}$ herein) is the least.

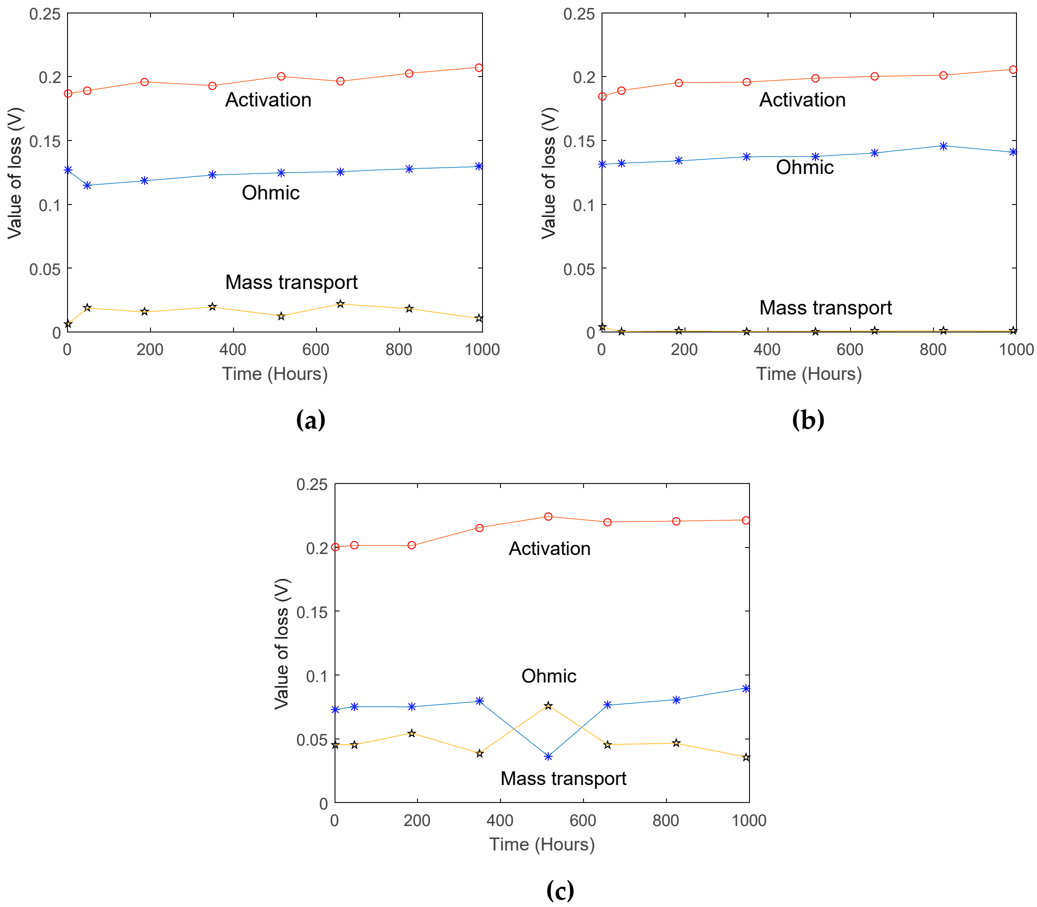


**Figure 5.** Evolution of three PEMFC losses during the test, using three different V-I models. (**a**) Equation (2); (**b**) Equation (3); (**c**) Equation (5).

Moreover, smaller mass transport loss from Equation (3) is further investigated. It is noted that Equation (3) cannot provide exact 'E' value at zero current. With Equation (3), when current approaches zero, the mass transport loss term tends to parameter 'm', not equal to zero. In order to solve this, the parameter 'm' has to be very small; as close as possible to zero. This can be expressed with Table 4, where model parameters at PEMFC normal states are obtained from three models. It can be seen that extremely small 'm' values can be obtained from Equation (3), in order to keep the model output to 'E' at zero current. Therefore, with extremely small 'm' values, small mass transport loss from Equation (3) can be provided; this restricts Equation (3) for expressing the actual mass transport variation in PEMFC.

However, variations can be observed from Figure 5 with different models. Firstly, as PEMFC voltage drop is larger than pre-defined failure threshold at 991 h, the PEMFC can be regarded as seriously degraded [22], but different variations are obtained with three V-I models from 823 h to 991 h, which are listed in Table 7. This can be further investigated using collected V-I curves at 823 h and 991 h, which are depicted in Figure 6a. It can be seen that Ohmic loss increases from 823 h to 991 h, while decreased mass transport loss is observed. This is consistent with the simulation results from Equation (5).

**Table 7.** Variations from 823 h to 991 h using three V-I models (varying trend and percentage is indicated using different arrows, ↑:increase; ↓:decrease; →: almost no variation).

| Model No. | Activation Loss (%) | Ohmic Loss (%) | Mass Transport Loss (%) |
|---|---|---|---|
| Equation (2) | ↑(2.22%) | →(1.33%) | ↓(41.4%) |
| Equation (3) | ↑(2.29%) | ↓(3.36%) | →(0%) |
| Equation (5) | →(0.402%) | ↑(11.2%) | ↓(22.5%) |

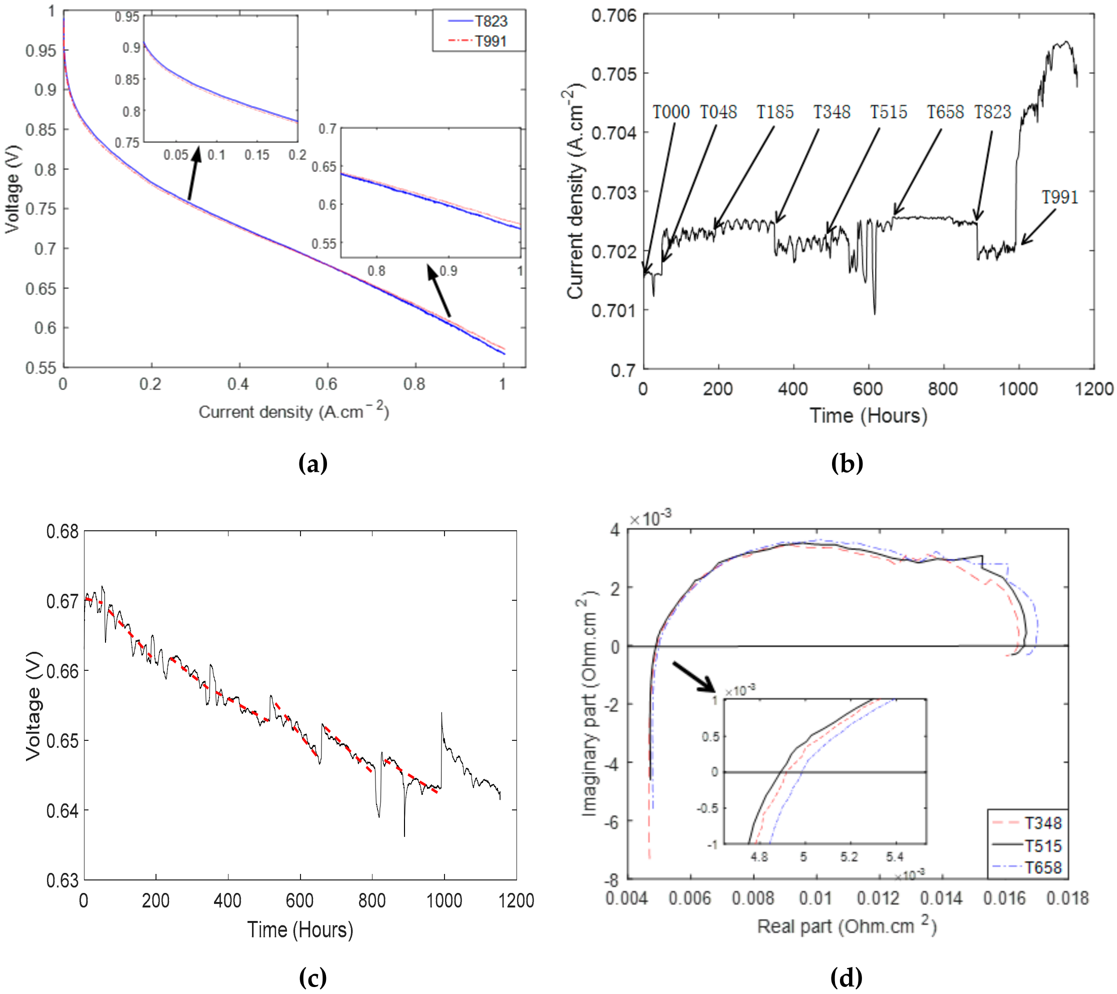


**Figure 6.** Tested PEMFC performance during the test. (**a**) Collected V-I curves at 823 h and 991 h; (**b**) Current density evolution; (**c**) Average cell voltage evolution; (**d**) Collected EIS at 348 h, 515 h and 658 h.

Moreover, it can also be found from Figure 5 that, with Equations (2) and (3), activation and Ohmic loss increases gradually with the PEMFC operation, while mass transport loss does not clearly show the trend. With Equation (5), however, a sudden change in PEMFC losses at 515 h is observed, where significant increased mass transport loss and decreased Ohmic loss are obtained. Therefore, it can be induced that the tested PEMFC stack experiences abnormal behavior at about 515 h using Equation (5).

The difference of interpreting PEMFC degradation using different models, i.e. normal operation at 515 h from Equations (2) and (3), and abnormal behavior at 515 h from Equation (5), is further studied. Figure 6b and c depict the evolution of current density and average cell voltage during the test, respectively. It should be noted that, in Figure 6c, the multi-linear curve fitting is applied to the average voltage, such that the degradation rate between consecutive polarization curve collections can be evaluated (shown as a red dashed line in Figure 6c). This is also listed in Table 8.

**Table 8.** PEMFC degradation rate at different time intervals during the tests.

| Time Period (h) | 0–48 | 48–185 | 185–348 | 348–515 | 515–658 | 658–823 | 823–991 |
|---|---|---|---|---|---|---|---|
| Degradation Rate ($\mu V \cdot h^{-1}$) | −38.84 | −37.81 | −24.79 | −28.43 | −50.99 | −37.87 | −28.26 |

From Figure 6b, although the constant control parameters listed in Table 1 are applied during the test, the current density does not show a strictly constant value, though a lower current density can be observed at 0 h, 515 h and 991 h. The PEMFC behavior at 0 h is due to the system warming up and does not express actual PEMFC performance, while at 991 h, the voltage decreases to the failure threshold, thus, PEMFC behavior at this point represent the failure performance. Therefore, the lower current density at 515 h should also represent PEMFC abnormal behavior; this is also consistent with Figure 6c and Table 7 that average cell voltage at 515 h shows a faster degradation rate. From previous studies, at PEMFC faulty state such as flooding or dehydration, the current density at flooded positions will decrease [28].

Moreover, the variation of Ohmic loss at 515 h is also investigated using the collected electrochemical impedance spectroscopy (EIS) data, which is depicted in Figure 6d. Based on previous studies [29], the intersection of the EIS curve and real axis represents the PEMFC internal resistance, which indicates the total Ohmic resistance of the PEMFC stack, especially the membrane resistance. It can be observed from Figure 6d that lower Ohmic resistance appears at 551 h, indicating reduced Ohmic loss at that time, which is consistent with the results from Equation (5).

Based on the above results, it can be concluded that Equation (5) can provide the best simulation performance, and the worst fitting is found from Equation (2), indicating that the use of exponential function for mass transport loss in V-I model can better simulate the PEMFC behavior, and with the modification of V-I model to account for OCV at zero current density, its simulation performance can be further improved. Moreover, with Equation (5), the PEMFC abnormal behavior can be detected by analyzing variations in different PEMFC losses, which further proves the necessity of considering PEMFC behavior at zero current density in the V-I model. This may be used in future studies of utilizing V-I model for PEMFC fault diagnosis.

## 4. Comparative Study of V-I Models in PEMFC Analysis at Faulty Conditions

In this section, the effectiveness of three V-I models in PEMFC analysis at faulty conditions, including flooding and dehydration, will be investigated. It should be noted that two different PEMFC systems are used to achieve flooding and dehydration, respectively, such that the robustness of V-I models in analyzing faulty behavior at different PEMFC systems can be better illustrated.

### *4.1. Description of Tested PEMFC Systems*

In this analysis, two different PEMFC systems are used to obtain test data at PEMFC faulty conditions, and the key technical details of tested PEMFC are listed in Table 9. Moreover, a single cell is used in these two tests.

**Table 9.** Technical details of two PEMFCs.

| Technical Parameter | PEMFC 1 | PEMFC 2 |
|---|---|---|
| **Thickness of Membrane (μm)** | 20 | 15 |
| **Electrode Area ($cm^2$)** | 25 | 25 |
| **Loading of Platinum ($mg \cdot cm^{-2}$)** | 0.15 @ anode, 0.35 @ cathode | 0.28 @ anode, 0.37 @ cathode |

It should be mentioned that two different testing systems and cells with different properties are used in this study. The reason is that with variations in the tested cells and PEMFC systems, the effectiveness of V-I models at different PEMFC applications can be investigated.

In the test, flooding and dehydration are achieved with two PEMFC systems, respectively. The flooding is caused by reducing the cell temperature, while the dehydration is caused by increasing the cell temperature and injecting dry gas reactants. This is listed in Table 10.

**Table 10.** Test set-up at two faulty conditions.

| **Test Set-up** | **PEMFC 1** | | **PEMFC 2** | |
|---|---|---|---|---|
| Control Parameter | Normal | Flooding | Normal | Dehydration |
| Cell Temperature (°C) | 45 | 30 | 60 | 70 |
| Relative Humidity (%) | 100 | 100 | 100 | 0 |

In each test, V-I curves are collected before and after the fault occurs, which are shown in Figure 7. It can be seen that, compared to polarization curves without faults, either flooding or dehydration can cause significant PEMFC performance decay. This is consistent with previous studies [25].

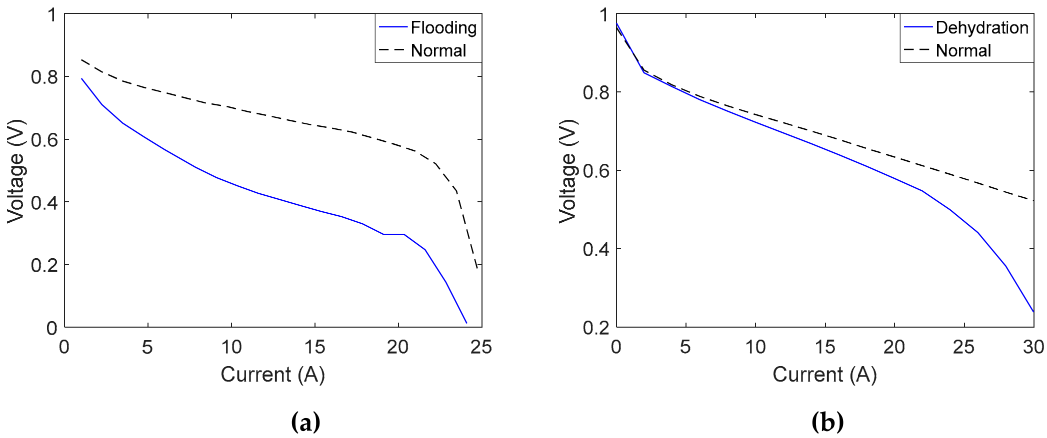


**Figure 7.** Collected V-I curves before and after the PEMFC faults occur. (**a**) Flooding; (**b**) Dehydration.

### *4.2. Effectiveness of V-I Models in Analyzing PEMFC Faults*

Similar to the analysis in Section 3.2, with collected V-I curves, three V-I models are applied to obtain the model parameters, from which simulation accuracy can be evaluated. Table 11 lists the simulation results of three V-I models at flooding and dehydration scenarios with RMSE.

**Table 11.** Simulation accuracy of three V-I models.

| **Model No.** | **Flooding @ PEMFC 1** | **Normal @ PEMFC 1** | **Dehydration @ PEMFC 2** | **Normal @ PEMFC 2** |
|---|---|---|---|---|
| Equation (2) | 0.01878 | 0.01663 | 0.01035 | 0.002825 |
| Equation (3) | 0.0145 | 0.01115 | 0.00833 | 0.002394 |
| Equation (5) | 0.01183 | 0.005456 | 0.00784 | 0.001458 |

It can be seen from Table 11 that, compared to the normal condition (as listed in Table 2), larger RMSE is provided when simulating PEMFC performance at faulty conditions with these three V-I models. However, since the maximum RMSE is below 0.02, the widely used V-I models can still provide reasonable simulation performance to actual PEMFC behavior.

Regarding simulation variation among three V-I models at PEMFC faulty conditions, similar results can be obtained as those at normal condition. Equation (5) can provide the best fitting performance, while the worst fitting is obtained with Equation (2). This also confirms that the expression of mass transport loss with exponential function can provide better simulation accuracy, which can be further improved by considering PEMFC behavior at zero current density in V-I model.

Furthermore, different PEMFC losses before and after the faults are calculated with three V-I models, thus, their performance in analyzing PEMFC faults can be investigated, the results are shown in Figure 8, where N, F and D represent normal, flooding and dehydration conditions, respectively.

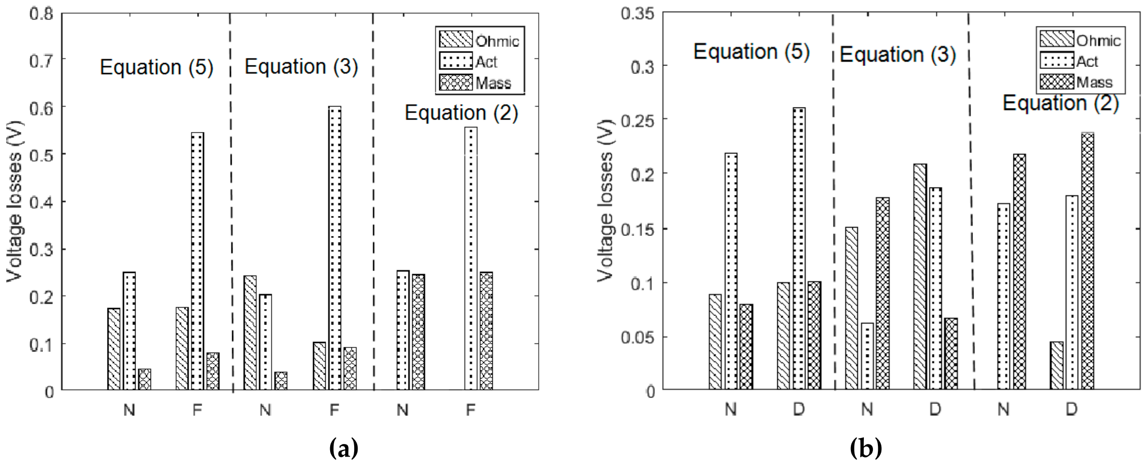


**Figure 8.** PEMFC losses before and after different faults occur. (**a**) Flooding; (**b**) Dehydration.

It can be observed from Figure 8a that at a flooding scenario, increased activation loss is obtained from all three V-I models, the reason is that flooding will inundate the catalyst and reduce the electrode activity, thus reducing the exchange current density '$i_0$' in the activation loss portion from which activation loss is increased. However, variation in Ohmic and mass transport losses is observed among three V-I models. Increased mass transport loss is found with Equations (3) and (5), while Equation (2) provides almost constant mass transport loss. Based on previous studies [24,25], gas channel or porous layers will be blocked at in flooding situation, leading to difficulty of mass transport within the PEMFC system, thus causing increase of mass transport loss. In the test, as the flooding scenario is clearly observed, and a significant PEMFC voltage drop is obtained due to flooding (as depicted in Figure 7a), it is concluded that interpretation from Equations (3) and (5) regarding mass transport loss change is more consistent with results from previous studies.

Regarding Ohmic loss, extremely small Ohmic loss before and after flooding is provided with Equation (2), since PEMFC is operated at a medium current range (10 A constant current in the test), as shown in Figure 6a, this range is within the linear range dominated by Ohimic resistance, thus the extremely small Ohmic loss is not reasonable. Moreover, a different variation in Ohmic loss is also found from Equations (3) and (5), where slightly increased Ohmic loss is obtained from Equation (5) and decreased Ohmic loss is found from Equation (3). Based on the previous studies [26,30], Ohmic resistance includes membrane resistance, electronic resistance of bipolar plates, and contact resistance between the bipolar plate and gas diffusion layer. Although membrane resistance will not be affected with accumulated liquid water, increased contact resistance can be induced, thus, the total Ohmic cell resistance will increase at the flooding state. Moreover, it can also be found from Figure 7a that the slope of Ohmic part after flooding is increased, further confirming increased Ohmic loss at flooding. Therefore, the effect of flooding on PEMFC Ohmic loss can be better illustrated with Equation (5).

From the above results, it can be seen that, when analyzing PEMFC internal behavior at flooding scenario, more consistent and reasonable results can be obtained with Equation (5), especially when interpreting mass transport and Ohmic loss variation due to the flooding. On the other side, inconsistent results are provided from Equation (2), indicating that the use of logarithm function for expressing PEMFC mass cannot interpret mass transport variation accurately in the flooding scenario.

Moreover, at dehydration state (Figure 8b), based on previous studies [25–27], Ohmic loss should increase, due to increased membrane resistance, and the dehydrated membrane will also reduce the catalyst reactions, leading to the increase of activation loss. Among analysis results from three V-I models, extremely small Ohmic loss is obtained from Equation (2), which is not reasonable, as PEMFC is operated within the range dominated by Ohmic resistance. Although both Equations (3) and (5) provide consistent Ohmic and activation loss variation with previous studies, different mass transport loss is obtained from two models, i.e. decreased mass transport loss is obtained from Equation

(3), and an increase in mass transport loss is observed from Equation (5). As shown in Figure 7b, mass transport loss becomes more serious after dehydration, thus the results from Equation (5) are more reasonable.

Based on above results, Equation (5) can still provide reasonable interpretations regarding PEMFC internal behavior at dehydration condition, in terms of variations in activation, Ohmic, and mass transport losses. However, it should be mentioned that, at the hydration scenario, reasonable mass transport change (increased mass transport loss due to dehydration) can be obtained. This further confirms that the inappropriate selection of V-I model may provide inconsistent interpretation of PEMFC internal behavior variation at different conditions, which is also the reason that only few studies have been devoted to PEMFC fault diagnosis using V-I models.

Therefore, it can be concluded that, when analyzing PEMFC performance at faulty scenarios (flooding and dehydration in this study), different interpretations of PEMFC internal behavior change can be provided using different V-I models, which makes it difficult to use V-I models in PEMFC applications. Results demonstrate that Equation (5) can provide the best simulation accuracy to the actual measurements, and also reasonable interpretations regarding PEMFC internal behavior change at both flooding and dehydration scenarios, while the other two models will show the inconsistent performance at these conditions.

It should be noted that although only flooding and dehydration are used in this study, the work can be easily expanded to other faulty scenarios. Therefore, with clarification of V-I model effectiveness in different PEMFC operating states, the use of V-I models in PEMFC analysis, including PEMFC fault diagnosis, can be favored by selecting appropriate V-I models at different applications.

In the future work, the more faulty testes will be performed to further validate the performance of Equation (5). Moreover, the effectiveness of using Equation (5) for PEMFC fault diagnosis will also be investigated.

## 5. Conclusions

In this paper, a comparative study is performed to investigate, the effectiveness of commonly used V-I models in simulating PEMFC behavior and analyzing its degradation process. In order to better illustrate the robustness of V-I models, three different PEMFC systems are used at normal and faulty scenarios.

From the results of analyzing PEMFC degradation at normal operation, the model using exponential function for mass transport loss and considering OCV at zero current can provide the best performance in terms of simulation accuracy and capability of identifying abnormal PEMFC behavior. Furthermore, a similar conclusion can be made when analyzing PEMFC performance at faulty scenarios; the most accurate simulation results can be achieved from Equation (5), and reasonable PEMFC loss variations due to flooding and dehydration can also be obtained with the same model. Therefore, when selecting appropriate V-I model in simulating and analyzing PEMFC behavior at different conditions, the model using an exponential function for mass transport loss expression should be used, and PEMFC behavior at zero current density should also be considered in the V-I model.

**Author Contributions:** Conceptualization, L.M. and X.C.; Methodology, L.M. and C.Z.; Software, C.Z.; Validation, L.M.; Formal Analysis, C.Z. and L.M.; Investigation, C.Z., W.L., and K.H.; Resources, L.M. and M.H.; Data Curation, C.Z. and W.L.; Writing-Original Draft Preparation, C.Z.; Writing-Review & Editing, C.Z. and L.M.; Visualization, C.Z. and W.L.; Supervision, L.M. and X.C.; Project Administration, L.M.; Funding Acquisition, L.M. All authors have read and agreed to the published version of the manuscript.

**Funding:** This work is supported by National Natural Science Foundation of China (NSFC) (51975549), State Key Laboratory of Mechanical System and Vibration (MSV202017), Anhui Provincial Natural Science Foundation (1908085ME161), and Natural Science Foundation of Shanghai (16ZR1417000).

**Conflicts of Interest:** The authors declare no conflict of interest.

## List of Symbols

| | |
|---|---|
| V | Fuel cell voltage (V); |
| E | Reversible cell voltage (V); |
| $\Delta V_a$ | Activation loss (V); |
| $\Delta V_o$ | Ohmic loss (V); |
| $\Delta V_m$ | Mass transport loss (V); |
| A | Tafel slope (V); |
| i | Current density ($A \cdot cm^{-2}$); |
| $i_0$ | Exchange current density ($A \cdot cm^{-2}$); |
| R | Fuel cell resistance ($\Omega \cdot cm^2$); |
| $\alpha i^k$ | Parameter act as 'amplification term' (V); |
| $\beta$ | Inverse of limiting current density ($cm^2 \cdot A^{-1}$); |
| B | Constant that depends on the fuel cell and its operating state (V); |
| $j_L$ | Limit current density at the cathode ($A \cdot cm^{-2}$). |
| m, n | Empirical parameters jointly determined by the operating conditions and the characteristics of the stack (V), ($cm^2 \cdot A^{-1}$); |
| $i_n$ | Electronic leakage current density ($A \cdot cm^{-2}$); |
| $C_1$ | Empirical parameters ($cm^2 \cdot A^{-1}$); |
| $y_i$ | *i*th test data of test (V); |
| $\overline{y_i}$ | *i*th fitting data of three V-I models (V); |
| N | Number of measurement data. |

## References


1. Mosaad, M.I.; Ramadan, H.S. Power quality enhancement of grid-connected fuel cell using evolutionary computing techniques. *Int. J. Hydrogen Energy* **2018**, *43*, 11568–11582. [CrossRef]
2. Priya, K.; Sathishkumar, K.; Rajasekar, N. A comprehensive review on parameter estimation techniques for Proton Exchange Membrane fuel cell modelling. *Renew. Sustain. Energy Rev.* **2018**, *93*, 121–144. [CrossRef]
3. Thosar, A.U.; Agarwal, H.; Govarthan, S.; Lele, A.K. Comprehensive analytical model for polarization curve of a PEM fuel cell and experimental validation. *Chem. Eng. Sci.* **2019**, *206*, 96–117. [CrossRef]
4. Blal, M.; Benatiallah, A.; NeCaibia, A.; Lachtar, S.; Sahouane, N.; Belasri, A. Contribution and investigation to compare models parameters of (PEMFC), comprehensives review of fuel cell models and their degradation. *Energy* **2019**, *168*, 182–199. [CrossRef]
5. Pessot, A.; Turpin, C.; Jaafar, A.; Soyez, E.; Rallières, O.; Gager, G.; Arbigny, J. Contribution to the modelling of a low temperature PEM fuel cell in aeronautical conditions by design of experiments. *Math. Comput. Simul.* **2019**, *158*, 179–198. [CrossRef]
6. Hou, Y.; Zhou, B.; Zhou, W.; Shen, C.; He, Y. An investigation of characteristic parameter variations of the polarization curve of a proton exchange membrane fuel cell stack under strengthened road vibrating conditions. *Int. J. Hydrogen Energy* **2012**, *37*, 11887–11893. [CrossRef]
7. El Aabid, S.; Régnier, J.; Turpin, C.; Rallières, O.; Soyez, E.; Chadourne, N.; d'Arbigny, J.; Hordé, T.; Foch, E. A global approach for a consistent identification of static and dynamic phenomena in a PEM Fuel Cell. *Math. Comput. Simul.* **2019**, *158*, 432–452. [CrossRef]
8. Bezmalinovic, D.; Simic, B.; Barbir, F. Characterization of PEM fuel cell degradation by polarization change curves. *J. Power Sources* **2015**, *294*, 82–87. [CrossRef]
9. Cai, C.; Rao, Y.; Zhang, Y.; Wu, F.; Li, S.; Pan, M. Failure mechanism of PEM fuel cell under high back pressures operation. *Int. J. Hydrogen Energy* **2019**, *44*, 13786–13793. [CrossRef]
10. Xia, L.; Zhang, C.; Hu, M.; Jiang, S.; Chin, C.S.; Gao, Z.; Liao, Q. Investigation of parameter effects on the performance of high-temperature PEM fuel cell. *Int. J. Hydrogen Energy* **2018**, *43*, 23441–23449. [CrossRef]
11. Mao, L.; Jackson, L.; Jackson, T. Investigation of polymer electrolyte membrane fuel cell internal behaviour during long term operation and its use in prognostics. *J. Power Sources* **2017**, *362*, 39–49. [CrossRef]
12. Babu, A.R.V.; Kumar, P.M.; Rao, G.S. Parametric study of the proton exchange membrane fuel cell for investigation of enhanced performance used in fuel cell vehicles. *AEJ Alex. Eng. J.* **2018**, *57*, 3953–3958. [CrossRef]

13. Vuppala, R.K.S.S.; Chedir, B.A.; Jiang, L.; Chen, L.; Aziz, M.; Sasmito, A.P. Optimization of membrane electrode assembly of PEM fuel cell by response surface method. *Molecules* **2019**, *24*, 3097. [CrossRef] [PubMed]
14. Salva, J.A.; Iranzo, A.; Rosa, F.; Tapia, E.; Lopez, E.; Isorna, F. Optimization of a PEM fuel cell operating conditions: Obtaining the maximum performance polarization curve. *Int. J. Hydrogen Energy* **2016**, *41*, 19713–19723. [CrossRef]
15. Squadrito, G.; Maggio, G.; Passalacqua, E.; Lufrano, F.; Patti, A. An empirical equation for polymer electrolyte fuel cell (PEFC) behaviour. *J. Appl. Electrochem.* **1999**, *29*, 1449–1455. [CrossRef]
16. Danilov, V.A.; Tade, M.O. An alternative way of estimating anodic and cathodic transfer coefficients from PEMFC polarization curves. *Chem. Eng. J.* **2010**, *156*, 496–499. [CrossRef]
17. Kim, J.; Lee, S.M.; Srinivasan, S. Modeling of proton membrane fuel call performance with an empirical equation. *J. Electrochem.* **1995**, *142*, 2670–2674. [CrossRef]
18. Guinea, D.M.; Moreno, B.; Chinarro, E.; Guinea, D.; Jurado, J.R. Rotary-gradient fitting algorithm for polarization curves of proton exchange membrane fuel cells (PEMFCs). *Int. J. Hydrogen Energy* **2008**, *33*, 2774–2782. [CrossRef]
19. Selyari, T.; Ghoreyshi, A.A.; Shakeri, M.; Najafpour, G.D.; Jafary, T. Measurement of polarization curve and development of a unique semi-empirical model for description of PEMFC and DMFC performances. *CI CEQ* **2011**, *17*, 207–214. [CrossRef]
20. FCLAB Research. IEEE PHM Data Chall 2014. Available online: http://eng.fclab.fr/ieee-phm-2014-data-challenge/ (accessed on 21 July 2020).
21. Hensel, J.P.; Gemmen, R.S.; Thornton, J.D.; Vipperman, J.S.; Clark, W.W.; Bucci, B.A. Effect of cell-to-cell fuel mal-distribution on fuel cell performance and a means to reduce mal-distribution using MEMS micro-valves. *J. Power Sources* **2007**, *164*, 115–125. [CrossRef]
22. Zhu, L.; Chen, J. Prognostics of PEM fuel cells based on Gaussian process state space models. *Energy* **2018**, *149*, 63–73. [CrossRef]
23. Wu, J.; Yuan, X.Z.; Martin, J.J.; Wang, H.; Zhang, J.; Shen, J.; Wu, S.; Merida, W. A review of PEM fuel cell durability: Degradation mechanisms and mitigation strategies. *J. Power Sources* **2008**, *184*, 104–119. [CrossRef]
24. Borup, R.; Meyers, J.; Pivovar, B.; Kim, Y.S.; Mukundan, R.; Garland, N.; Myers, D.; Wilson, M.; Garzon, F.; Wood, D.; et al. Scientific aspects of polymer electrolyte fuel cell durability and degradation. *Chem. Rev.* **2007**, *107*, 3904–3951. [CrossRef] [PubMed]
25. Schmittinger, W.; Vahidi, A. A review of the main parameters influencing long-term performance and durability of PEM fuel cells. *J. Power Sources* **2008**, *18*, 1–14. [CrossRef]
26. Zheng, Z.; Luo, L.; Zhu, F.; Cheng, X.; Yang, F.; Shen, S.; Wei, G.; Zhang, J. Degradation of core-shell Pt3Co catalysts in proton exchange membrane fuel cells (PEMFCs) studied by mathematical modelling. *Electrochim. Acta* **2019**, *323*, 134751. [CrossRef]
27. Rama, P.; Chen, R.; Andrews, J. A review of performance degradation and failure modes for hydrogen-fueled polymer electrolyte fuel cells. *Proc. Inst. Mech. Eng. A J. Power Energy* **2008**, *222*, 421–441. [CrossRef]
28. Ifrek, L.; Chadebeck, O.; Rosini, S.; Cauffet, G.; Bultel, Y.; Bannwarth, B. Fault identification on a fuel cell by 3-D current density reconstruction from external magnetic field measurement. *IEEE Trans. Magn.* **2019**, *55*, 6200705. [CrossRef]
29. Zheng, Z.; Pera, M.C.; Hissel, D.; Becherif, M.; Agbli, K.S.; Li, Y. A double-fuzzy diagnostic methodology dedicated to online fault diagnosis of proton exchange membrane fuel cell stacks. *J. Power Sources* **2017**, *271*, 570–581. [CrossRef]
30. Nunez-Toledo, L.E.; Castaneda, S.; Orozco-Gallo, D.C.; Ribadeneira, R. PEMFCs multiscale modelling: Determination of overpotential with description of electron transfer in cathodic EDL at different O2 concentrations. *Electrochim. Acta* **2020**, *331*, 135361. [CrossRef]